Available online at www.sciencedirect.com
SCIENCE DIRECT®
PERGAMON
International Journal of Heat and Mass Transfer 46 (2003) 1199–1213
International Journal of HEAT and MASS TRANSFER
www.elsevier.com/locate/ijhmt

Experimental and numerical analysis of the temperature transition of a suspended freezing water droplet

J.P. Hindmarsh *, A.B. Russell, X.D. Chen

Department of Chemical and Materials Engineering, The University of Auckland, Private Bag 92019, Auckland, New Zealand

Received 11 May 2001; received in revised form 27 August 2002

Abstract

The objective of this study was to develop a simple experimental and numerical method to study the temperature transition of freezing droplets. One experimental approach and several numerical methods were explored. For the experimental method, a droplet was suspended in a cold air stream from the junction of a thermocouple. The droplet's temperature transition was able to be accurately measured and the freezing of the droplet observed. The numerical models developed were able to predict the temperature transition and the freezing time of the droplet. Of the numerical methods, a simple heat balance model was determined to be an accurate means of predicting the freezing time of the droplet.

Keywords: Freezing transitions; Freezing time prediction; Suspended droplet; Moving boundary problem; Supercooled

1. Introduction

The temperature transition of a freezing droplet is of major importance to the study of spray crystallization processes. Spray crystallization is a newly developed process for crystallization of food stuffs. It can be simply described as the solidification of a liquid by atomization into a cold atmosphere [1]. Being able to predict the cooling and freezing times of droplets is essential to optimizing refrigeration requirements and for anticipating the microstructure of a frozen droplet.

This study was the first step towards developing an experimental method to measure the temperature transition in the freezing of droplets of solutions. The aim was to develop numerical models which would simulate observed experimental results in order to predict freezing times and solute redistribution for different freezing conditions. The first step involved only the freezing of distilled water, so that the numerical predictions of the temperature transition and freezing times could be validated experimentally prior to solute redistribution being incorporated into the model.

Most of the development of experimental methods for single droplets has arisen as a result of studies of the drying kinetics of various liquid suspensions. There are two types of experimental techniques for the study of single droplets: free flight and levitation. Free flight studies involve allowing a droplet to free fall, then measuring time dependent variables either by observation or by catching the droplet at different drop heights [2].

Levitation involves the droplet remaining stationary whilst air is flowed past it. Levitation techniques can either be non-intrusive or intrusive. Non-intrusive levitation employs various physical forces to freely levitate the droplet. This can be achieved with acoustic, electromagnetic [3], electrostatic [4] or aerodynamic forces [5]. One of the more unusual approaches is optical levitation by lasers [6].

While non-intrusive methods have the advantage of better approximating actual conditions, the experimental apparatus required is generally expensive. Further, difficulties arise in accurately measuring the temperature

* Corresponding author. Present address: Department of Chemical Engineering, University of Cambridge, Pembroke Street, Cambridge CB2 3RA, UK. Tel.: +44-0-1223-766339; fax: +44-0-1223-334796.

E-mail address: jph47@cam.ac.uk (J.P. Hindmarsh).

0017-9310/03/$ - see front matter
PII: S0017-9310(02)00399-X

Nomenclature

c	specific heat capacity ($J\,kg^{-1}\,K^{-1}$)
D_{ab}	air/water vapour diffusivity ($m^2\,s^{-1}$)
E_v	crystal growth activation energy ($J\,kg^{-1}$)
f	solid front position (m)
h	heat transfer coefficient ($J\,s^{-1}\,m^{-2}\,K^{-1}$)
h_m	mass transfer coefficient ($m\,s^{-1}$)
k	thermal conductivity ($W\,m^{-1}\,K^{-1}$)
K_m	kinetic coefficient ($m\,s^{-1}\,K^{-1}$)
l_{th}	exposed length of thermocouple (m)
L	latent heat of phase change ($J\,kg^{-1}$)
Nu	Nusselt number
Pr	Prandtl number
q	heat flux ($J\,m^{-2}$)
r	radial coordinate (m)
R	droplet radius (m)
R_c	universal gas constant ($J\,kg^{-1}\,K^{-1}$)
Re	Reynolds number
Sc	Schmidt number
Sh	Sherwood number
t	time (s)
T	temperature (°C)
T_a	ambient temperature (°C)
T_f	equilibrium freezing temperature (°C)
T_{int}	initial droplet temperature (°C)
T_n	nucleation temperature (°C)
v	ambient air velocity ($m\,s^{-1}$)
V_d	volume of droplet (m^3)
V_f	volume of droplet frozen (m^3)

Greek symbols

α	thermal diffusivity ($m^2\,s^{-1}$)
ϵ	emissivity
ϑ	interface velocity ($m^3\,s^{-1}$)
μ	viscosity (Pa s)
ρ	density ($kg\,m^{-3}$)
σ	Stefan–Boltzmann constant

Subscripts

a	ambient air
e	evaporation
d,s	droplet surface
f	fusion
h	heat transfer
i	solid/liquid interface
l	liquid phase
m	mass transfer
r	thermal radiation
s	solid phase
sb	sublimation
th	thermocouple
v	vapor phase

of the droplet. El-Kaddah and Szekely [3] and Song and Li [7] have undertaken pioneering work into numerically modelling the heat transfer and internal fluid flow of levitated droplets.

Intrusive methods involve suspending a droplet on a thin mesh or plate, the tip of a glass filament or the junction of a thermocouple [5,8]. The suspension of droplets on thermocouples has been successfully used in the past for freezing studies [9,10] whilst the development of fine fast response thermocouples and high-speed data acquisition systems now offers an inexpensive and uncomplicated method of accurately measuring the temperature transition of a droplet. Lin and Chen [11] developed a simple experimental apparatus to measure the temperature transition of drying droplets whilst suspended on a thermocouple. Substitution of the heated air stream with a cold air stream enabled their technique to be adapted for the purposes of this particular study.

In order to develop a numerical model of the freezing process, an accurate physical description of the process was initially required. The freezing process of a droplet can be described in four distinct stages [12–14]:

(1) A pre-cooling or supercooling stage, during which the liquid droplet is cooled from an initial temperature to below the equilibrium freezing temperature, until crystal nucleation occurs.
(2) A recalescence stage, during which supercooling drives rapid kinetic crystal growth from the crystal nuclei. This stage is terminated when the supercooling is exhausted and the droplet has reached its equilibrium freezing temperature.
(3) A freezing stage, where crystal growth is governed by the heat transfer rate from the droplet to the point where the droplet liquid is completely frozen.
(4) A cooling or tempering stage, where the solid droplet temperature is reduced to near the ambient air temperature.

Fig. 1 shows an idealized temperature transition of the four stages of a freezing droplet. In order to develop a numerical model, each stage of the freezing process had to be described separately. The prediction of the temperature transition of each stage was undertaken by balancing the internal energy of the droplet against the heat loss to the environment. Established methods of modelling heat and mass transfer were employed in this particular study.

Heat transfer from droplets has been studied extensively both experimentally and theoretically. Yao and Schrock [15] provide a helpful summary of early re-

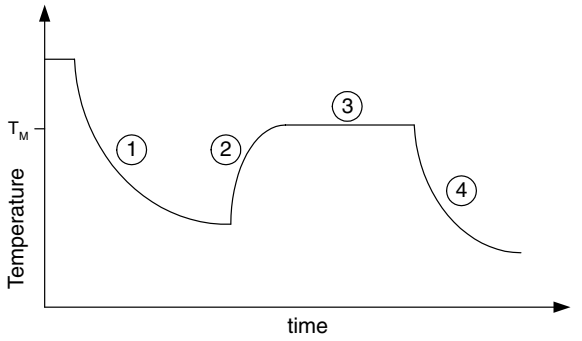

Fig. 1. The temperature transition of the four stages of freezing of a droplet.

search on this topic and present a methodology for modelling heat and mass transfer from droplets. They postulate that for cooling of airborne droplets in a cold atmosphere, heat transfer occurs by three main mechanisms: convective heat transfer, convective mass transfer and thermal radiation from the droplet surface. They also demonstrate two ways to model the internal heat transfer of a droplet: one by solving the internal temperature profile by describing internal heat conduction and the other by assuming a uniform temperature within the droplet. The assumption of a uniform temperature meant that the transient heat transfer of the droplet could be predicted by simply balancing the heat flux from the surface by heat and mass transfer with the internal energy of the droplet [15]. Yao and Schrock [15] concluded that the uniform temperature within a droplet was a product of internal mixing of liquid within the droplet.

Uniform temperature assumptions have also been used to predict freezing times of droplets in studies of artificial snowmaking methods [16]. However, with those methods, only a simple energy balance was needed to model the freezing stage. This simply involved the balancing of the external heat transfer with the amount of latent heat required to be removed in order to completely freeze the mass of water in the droplet.

The uniform temperature method was used in this particular study. However, in order to assess the validity of the uniform temperature assumption, a further model was formulated to solve the internal spatially distributed temperature profile of the droplet at all stages of the freezing process.

The internal temperature profile during the cooling stages (1) and (4) can be solved with a simple finite difference description of the transient heat conduction equations, using boundary conditions to describe the external heat fluxes from the droplet. The heat transfer driven freezing stage (3) is a Stefan type problem which requires the dual solution of the temperature distribution and freezing front position of the solidifying droplet. This is generally called a "moving boundary problem" [17].

A multitude of formulation methods have been previously devised to solve the moving boundary problem. Below is a list of methods available; the detailed description of the numerical formulation can be found in the appropriate references:

(a) Temperature formulation, Murry and Landis [18].
(b) Enthaply formulation, Voller [19].
(c) Heat balancing integral methods, Caldwell and Chan [20].
(d) Equivalent heat capacity method, Bonacina [21].
(e) Crystal growth method, Wang and Matthys [22].
(f) Most recently developed thermodynamic formulation called the phase field method, Wheeler and Ahmad [23].

The partial differential equations of these formulations can be discretized with the explicit difference formulae, the fully implicit, or two or three time level implicit solutions on either fixed grids or deforming grids [24]. Each method offers either one or more advantages. The explicit temperature or enthalpy methods are preferable for ease of formulation and minimal computation time. Levi [25] used the enthalpy method to model the heat flow in atomized metal droplets. The three time step equivalent heat capacity method is considered the most accurate prediction of the temperature transition, especially for multi-component solutions with varying freezing temperatures, such as foodstuffs [24,26].

The temperature method expressed on a deforming grid is by far the most accurate way to predict the solid/liquid interface position. It has been applied to solving the solidification of metal and organic droplets [12,13]. It is advantageous for the solution of coupled heat and mass transfer, such as solidification of metal alloys [27]. The crystal growth, heat balancing integral and phase field methods have the advantage of being able to be applied to non-equilibrium solidification. The crystal growth [22] and heat balancing integral methods [12] have been applied to solve the rapid solidification from supercooled melts. The phase field method has been used to analyse solidification on a micro-scale, such as dendrite growth in metallic systems [28].

In choosing a formulation method and grid, thought was given to which method would most correctly describe the type of solidification occurring. For the experimental method used in this study, the suspension of the droplet on a thermocouple added a complication to the formulation of the moving boundary model. Because of the inclusion of the thermocouple into the droplet, it was supposed that heterogeneous nucleation would most likely initiate at the liquid/thermocouple interface. Therefore, the droplet would freeze from the center

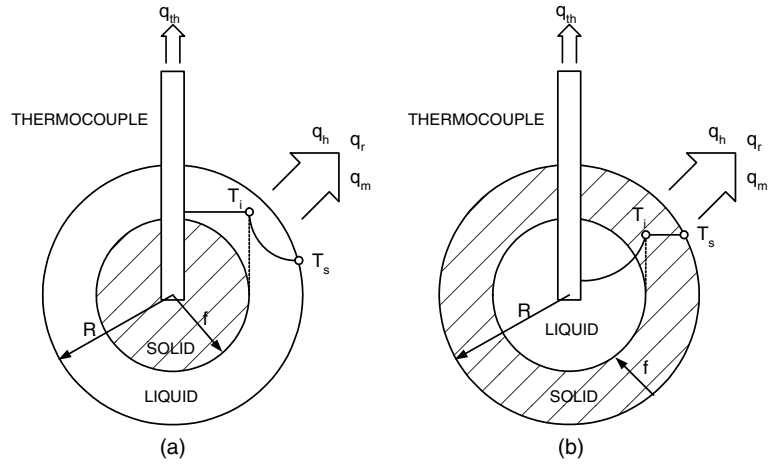

Fig. 2. Schematic diagram of freezing droplet: (a) outward freezing from initial frozen center; (b) inward freezing from initial frozen shell.

outward. Heat would thus be conducted away from the solid/liquid interface through an undercooled melt. This process is illustrated in Fig. 2(a). However, previous experimental studies have observed that droplets generally nucleate at the surface forming a frozen shell which propagates inwardly [29,30] (see Fig. 2(b)). Thus, most of the previous numerical treatments of freezing droplets referred to above were formulated to only solve the inward moving boundary situation [12,20,26]. Therefore, a method which had not been adapted for droplets before was needed to solve the outward moving boundary situation. The enthalpy and equivalent heat capacity methods were not considered as they are unable to accommodate melt undercooling without adjustment of the formulation [14]. Brunier et al. [13] and Wang et al. [27] modelled solidification from a supercooled melt with a temperature formulation on a deforming grid. This method offers an accurate prediction of the temperature profile and interface position. It can also be easily adapted to include mass transfer. Models describing both inward and outward freezing were thus formulated and compared against experimental results.

2. Experimental

Experiments were conducted to measure the temperature transition within freezing droplets of water. Described simply, a droplet was suspended on a thermocouple in a cold air stream while the temperature at the thermocouple tip was recorded. A schematic diagram of the experimental rig is shown in Fig. 3.

The droplet was suspended on thermocouple 1 in Fig. 3. This was a 25.4 μm diameter T-type copper–constantan thermocouple (Omega Inc., UK). The air stream temperature was monitored with thermocouples 2 and 3. These were 1 mm diameter T-type thermocouples (Omega Inc., UK). All thermocouples were sampled at 50 Hz by a Keithley DAS800/EXP16-A data recorder. The temperatures were monitored and recorded on a personal computer with Labtech Notebookpro software (Labtech Technologies Corporation, USA).

A twin-fluid nozzle was used to mix liquid nitrogen with dry air to produce a cold air stream. This was then used to cool another air stream. The advantage of using two air streams was that it enabled independent control of the air flow rate and temperature. Each air stream had the moisture scrubbed from it with beds of silica gel.

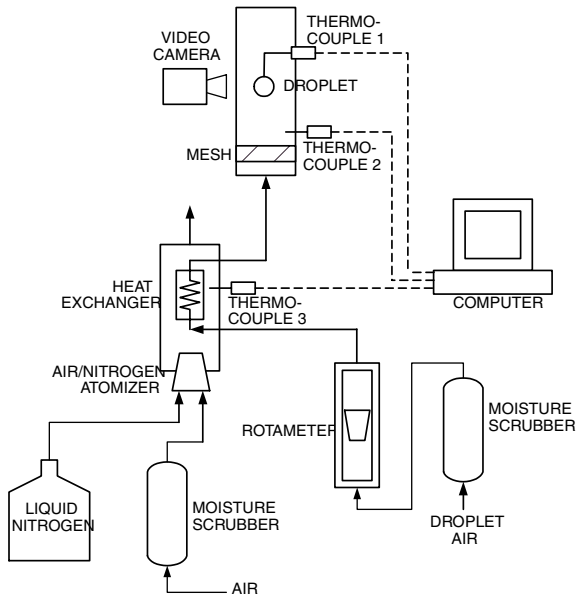

Fig. 3. Schematic diagram of experimental rig.

Table 1
Range of experimental parameters

Parameter	Experimental range
Air temperature (T_a)	−30 to −15 °C
Nucleation temperature (T_n)	−21 to −3 °C
Air velocity (v)	0.42–0.97 (m s^{-1})
Droplet size	0.5–2 μl ($R = 0.49$ to 0.78 mm)

This was done to avoid blockage through icing and uncontrolled nucleation of the droplet by airborne ice particles. A rotameter was used to measure the air flow rate.

Each experiment initially required the freezing air stream to be stable. The droplet air flow was set at a constant rate and redirected away from the droplet. The air and liquid nitrogen flows were adjusted until the droplet air temperature (thermocouple 3) was stable. A 5 μl micro-syringe was then used to place a droplet of distilled water on the junction of thermocouple 1. The junction of the thermocouple was approximately positioned at the center of the droplet by attaching a ball of glue half a diameter above the junction of the thermocouple wire from which the droplet was suspended. The temperatures were recorded until the droplet was completely frozen and cooled to the ambient air temperature.

A video camera with high magnification macro lenses was used to record the freezing of the droplet. The droplet nucleation temperature was adjusted by gluing on the thermocouple junction a small piece of silver iodide powder prior to placing the droplet on the thermocouple. This acted as an ice nucleating agent and initiated nucleation at a warmer temperature.

All of the thermocouples were calibrated at the freezing point of distilled water to ±0.2 °C. The air temperature was controlled to within ±0.5 °C The rotameter air velocity was calibrated with a hot-wire anemometer to ±0.02 m s^{-1}. The micro-syringe had a droplet size deviation of 0.01 μl. For the minimum settings of the experimental parameters (see Table 1) the total experimental uncertainty was ±6%.

3. Numerical models

Physical models can be developed by balancing the internal energy with the heat flux from the droplet. The external heat fluxes from the droplet are shown in Fig. 2. The temperature transition of the droplet is then solved by balancing the internal energy with the energy removed by heat transfer q_h, mass transfer q_m, thermal radiation q_r from the surface and heat conduction through the thermocouple q_{th}.

For the freezing process, the governing equations describing the internal heat balance of the droplet and the physical properties are discontinuous for the four stages (liquid to solid). It is therefore convenient to formulate a separate model for the internal heat balance of each stage. The cooling stages (1 and 4) and the freezing stage (3) can be modelled by assuming a uniform temperature or by solving the internal heat conduction of the droplet.

For each stage, the models were evaluated against the experimental results to determine the best method to be used to predict the freezing times of water droplets.

3.1. Surface heat fluxes

The convective heat flux q_h from the droplet surface is described by

$$q_h = h(T_{d,s} - T_a) \tag{1}$$

And the heat flux q_m due to convective mass transfer is

$$q_m = Lh_m(\rho_{vd,s} - \rho_{va}) \tag{2}$$

where L is the latent heat of phase change, either evaporation or sublimation. For dual heat and mass transfer from a sphere, Ranz and Marshall developed the following correlations for the Nusselt number Nu and Sherwood number Sh [31] to estimate the heat and mass transfer coefficients h and h_m:

$$Nu = \frac{2hR}{k_a} = 2 + 0.6Pr^{1/3}Re^{1/2} \tag{3}$$

$$Sh = \frac{2h_mR}{D_{ab}} = 2 + 0.6Sc^{1/3}Re^{1/2} \tag{4}$$

where R is the droplet radius, the vapour–air diffusivity is D_{ab}, the air thermal conductivity is k_a, and Re is the Reynolds number. For flow past a sphere the latter is given by

$$Re = \frac{2R\rho_a v}{\mu_a} \tag{5}$$

where v, ρ_a, μ_a are the air velocity, density and viscosity respectively. The Schmidt number, Sc is

$$Sc = \frac{\mu_a}{\rho_a D_{ab}} \tag{6}$$

and the Prandtl number, Pr is given by

$$Pr = \frac{\mu_a}{\rho_a \alpha_a} \tag{7}$$

where α_a is the thermal diffusivity of the air. For air below 0 °C Pr is approximately constant at 0.7 [9].

Also the heat flux q_r due to thermal radiation was

$$q_r = \epsilon\sigma(T_{d,s}^4 - T_a^4) \tag{8}$$

where ϵ is the emissivity for thermal radiation and σ is the Stefan–Boltzmann constant for thermal radiation.

3.2. Heat flux through thermocouple wire

Fig. 2 shows that the effect of the thermocouple is not symmetrical. To maintain a one-dimensional model, the thermocouple was estimated as a single point heat flux from the center of the droplet. The thermocouple is represented by a finitely long fin of length l_{th}, where l_{th} is the length of thermocouple exposed to the ambient air. The heat flux through the thermocouple q_{th} is thus [31]:

$$q_{th} = \sqrt{\frac{\pi^2}{32} R^3 k_{th} h_{th} (T_{d,s} - T_a)} \tanh\left(\sqrt{\frac{16h}{Rk_{th}}} l_{th}\right) \quad (9)$$

A general correlation for convection from a cylinder was used to find the heat transfer coefficient h_{th} for the exposed thermocouple wire [31].

3.3. Cooling stages

The internal energy balance of the solid and liquid cooling stages (stages 1 and 4) can be solved by assuming a uniform temperature distribution or solving the internal heat conduction. The temperature transition and cooling times (time from one temperature to another) of the droplet were predicted with the models.

Some physical properties of water/ice (density ρ, heat capacity c and thermal conductivity k) change with temperature. Incorporating functions to estimate the changing properties adds complexity to the models whilst in some cases not significantly increasing the accuracy of the model. So, for both the liquid and solid cooling stages, models were trailed using constant properties, whilst others had functions incorporated estimating the changing of properties for different temperatures. For the constant property model, the properties of water and ice were evaluated at 0 °C. For the changing properties model, polynomial equations were fitted to published data [32–34]. The physical properties and equations used for model predictions are detailed in Table 2.

3.3.1. Uniform temperature solution

Assuming a uniform temperature of the droplet, for cooling of the liquid and the solid droplet (stages 1 and 4) the temperature transition can be calculated by the heat balance:

$$c\rho V_d \frac{dT_d}{dt} = q_h + q_m + q_r + q_{th} \quad (10)$$

A forward difference time discretization was used to solve the transient droplet temperature. For each time step, the droplet volume was recalculated to compensate for the volume change due to mass transfer.

Table 2
Physical properties of water, ice and air used for numerical predictions

Parameter	Units	Value or prediction method
T_f	°C	0[a]
k_l	$J\,m^{-1}\,s^{-1}\,K^{-1}$	0.569[a](at 273 K)
k_s	$J\,m^{-1}\,s^{-1}\,K^{-1}$	2.26[a](at 273 K) & $-0.011T + 5.22$[b]
k_a	$J\,m^{-1}\,s^{-1}\,K^{-1}$	$7.61 \times 10^{-5}T + 3.48 \times 10^{-3}$[b]
c_l	$J\,kg^{-1}\,K^{-1}$	4217[a](at 273 K) & $-0.0011T^3 + 0.732T^2 - 163T + 16582$[b]
c_s	$J\,kg^{-1}\,K^{-1}$	2116[a](at 273 K) & $7.178T + 141$[b]
L_e	$J\,kg^{-1}$	2.502×10^6[a]
L_f	$J\,kg^{-1}$	3.33×10^5[a]
L_s	$J\,kg^{-1}$	2.838×10^6[c]
ρ_l	$kg\,m^{-3}$	999.8[a](at 273 K) & $-0.02T^2 + 10.8T - 470$[d]
ρ_l	$kg\,m^{-3}$	916.7[a](at 273 K) & $-0.163T + 961.4$[d]
ρ_a	$kg\,m^{-3}$	$-0.00513T + 2.69$[a]
ρ_{vo}	$kg\,m^{-3}$	0.00484731 (at 273 K)[e]
ρ_v	$kg\,m^{-3}$	$(1/\rho_{vo})\exp^{-0.0773T_a}$[e]
μ_a	$N\,s\,m^{-2}$	$5.0 \times 10^{-8}T + 3.46 \times 10^{-5}$[e]
D_o	$m^2\,s^{-1}$	0.000022 (at 273 K)[e]
D_{ab}	$m^2\,s^{-1}$	$D_o[(273 + T_{d,s})/273]^{1.853}$[e]
K_m	$m\,s^{-1}\,K^{-1}$	0.0028[c]
Pr_a	–	0.72[c]

[a] Perrys and Green [34].
[b] Kucherov (fit of data 203–273 K) [32].
[c] Hobbs [9].
[d] CRC (fit of data 247–273K) [33].
[e] Dorsey [40].

3.3.2. Internal heat conduction model

It was assumed that the droplet shape was constant and spherical and therefore it could be described with a one-dimensional model. The temperature formulation of the transient one-dimensional heat conduction in a spherical droplet is described by [13]

$$c\rho\frac{\partial T}{\partial t}=\frac{\partial}{\partial r}\left(k\frac{\partial T}{\partial r}\right)+\frac{2k}{r}\frac{\partial T}{\partial r} \tag{11}$$

At the droplet surface ($r=R$) the boundary condition was the sum of the heat fluxes q_h, q_m and q_r.

$$-k\left.\frac{\partial T}{\partial r}\right|_{r=R}=q_h+q_m+q_r \tag{12}$$

At the center of the droplet ($r=0$) the boundary condition was the heat flux through the thermocouple q_{th}.

$$-k\left.\frac{\partial T}{\partial r}\right|_{r=0}=q_{th} \tag{13}$$

3.4. Recalescence stage

For a droplet with a large undercooling at the time of nucleation, the temperature transition occurs extremely rapidly until the droplet reaches the equilibrium freezing temperature. A global heat balance can be used to estimate the frozen volume produced from the recalescence. The mass of water frozen is such that the latent heat released raises the droplet temperature to the equilibrium freezing temperature T_f [9,35,36]. Therefore, the volume of solid produced from nucleation is estimated by

$$V_f=V_d\frac{c_l\rho_l}{\rho_s}\frac{(T_f-T_n)}{L_f} \tag{14}$$

The nucleation temperature T_n was taken from experimental results. On reaching T_n the droplet was assumed to instantly change to the equilibrium freezing temperature T_f and be partially frozen volume V_f.

3.5. Freezing stage

After nucleation produces a partially frozen volume fraction V_f, the freezing of the remaining liquid was controlled by the rate of heat transfer from the droplet. How the internal heat transfer of the droplet is solved depends on what assumption was made of the form of the ice volume V_f produced by nucleation:

(a) *Heat balance model*: solid fraction is uniformly spread throughout the droplet as a fine dendritic structure. Solid fraction increases uniformly within the droplet as the latent heat of fusion was removed by external heat fluxes.

(b) *Outward moving boundary model*: solid core at the center of the droplet which grows outwardly to the surface. External heat fluxes conduct heat though undercooled liquid to droplet surface.

(c) *Inward moving boundary model*: solid shell on the surface which grows inwardly to center. External heat fluxes conduct heat though solid to droplet surface.

3.5.1. Heat balance model

The droplet freezes at a constant temperature T_f (stage 3) and the rate at which the solid (frozen) volume increases is calculated from the heat balance:

$$L_f\rho_s\frac{dV_f}{dt}=q_h+q_m+q_r+q_{th} \tag{15}$$

It was assumed that the outer surface of the droplet was liquid while freezing, so, mass transfer from the surface was by evaporation. Eq. (15) was solved with a forward difference time step. For each time step, the droplet size was updated to compensate for the liquid loss by mass transfer.

3.5.2. Moving boundary models

A schematic diagram of the outward and inward freezing of a droplet is illustrated in Fig. 2. It was assumed that the solid/liquid boundary was a clearly defined interface located at radius f, which propagated at a velocity $v=df/dt$ from or towards the center of the droplet.

After the recalescence stage, the droplet temperature was at T_f and the initial location of the interface for the freezing stage was calculated by rearrangement of Eq. (14). For outward freezing the initial position of solid/liquid interface was

$$f_i=R\sqrt[3]{V_f} \tag{16}$$

and for inward freezing

$$f_i=R\sqrt[3]{1-V_f} \tag{17}$$

The droplet was fully frozen once the interface f had propagated the radius of the droplet. The interface velocity ϑ was driven by the temperature gradient at the phase front and was defined by the additional boundary condition at the solid/liquid interface ($r=i$):

$$\rho_s L_f\frac{df}{dt}=k_s\left.\frac{\partial T_s}{\partial r}\right|_{(r=i)}-k_l\left.\frac{\partial T_l}{\partial r}\right|_{(r=i)} \tag{18}$$

For inward freezing, the solidification takes place at the equilibrium freezing temperature T_f. The interface velocity was then directly determined by the energy balance Eq. (18) and depended on the temperature gradient at the phase front. The variable space network given by Murray and Landis [18] was used. A fully implicit scheme of Eqs. (11)–(13) was solved with a

tri-directional matrix algorithm and the phase boundary location updated explicitly with Eq. (18).

For outward solidification the heat transfer was through an undercooled melt therefore the interface velocity was dependent on the kinetic growth rate of ice. The kinetic crystal growth depends on molecular mechanisms. For crystal growth from a pure melt, the interface velocity can be modelled by [22]

$$\vartheta = \vartheta_0 \exp\left[-\frac{E_v}{RT_f}\frac{T_f - T_i}{T_i}\right]\left[1 - \exp\left(-\frac{L_f}{R_c T_f}\frac{T_f - T_i}{T_i}\right)\right] \tag{19}$$

where ϑ_0 is the molecular attachment velocity ($m\,s^{-1}$), E_v the activation energy ($J\,kg^{-1}$) and R_c the universal gas constant. For a small undercooling, Eq. (19) reduces to the following linear approximation [22]:

$$v = K_m(T_f - T_i) \tag{20}$$

where K_m, the kinetic coefficient ($m\,s^{-1}\,K^{-1}$) can be estimated from experimental measurements of the growth velocity of ice from bulk undercooled water [9].

With Eq. (20) there are two unknown parameters at the solid/liquid interface: the interface velocity ϑ and the interface temperature T_i. Therefore, an iteration scheme was required to obtain a solution. The technique prescribed by Wang et al. [27] was used. An implicit Murray and Landis [18] scheme was also used to solve the temperatures for each kth iteration and the interface location updated with Wang's scheme. The convergence criteria for each time step was

$$\left|\frac{\Delta\vartheta^k}{\vartheta^k}\right| < 0.001 \tag{21}$$

The temperature indicated by the thermocouple was not a point temperature but an average temperature of a body of water surrounding the junction. The droplet center temperature predicted by the model was an average over a volume at the center of the droplet which would have produced the detectable temperature difference of 0.2 °C at the junction.

3.6. Freezing time prediction

An accepted definition of the freezing time is the point of time from the onset of cooling until the center temperature reaches −10 °C [37]. A model combining all the four stages of freezing was thus required to predict the freezing time of a droplet. The liquid and solid cooling stage models were evaluated separately against experimental liquid/solid cooling times. The most accurate of the liquid and solid cooling models was combined with the recalescence model together with all the proposed freezing stage models to evaluate the performance of the combined models for predicting the experiential freezing times.

4. Numerical solutions

All models were programmed in Matlab version 6.0 (Mathworks, USA). To ensure the numerical results were time step and grid independent, the time step and spacial grid settings were decreased until the solutions were stable with less than 0.01% variation from the previous larger setting. A time step of 0.02 s was used for all the cooling models. For the finite difference models, 40 nodes were required. The freezing stages for both moving boundary models were solved with 40 nodes for each region with a time step of 0.01 s.

5. Results and discussion

5.1. Experimental results

An example of the transient temperature of a freezing droplet is shown in Fig. 4. The four stages of freezing can be clearly seen. Once exposed to the cold ambient air (time zero) the temperature of the droplet reduced until the water nucleated (−13.5 °C on Fig. 4). At nucleation, recalescence occurs, the latent heat released from crystallization raises the droplet temperature to the equilibrium freezing temperature (0 °C for water). The temperature remains at the equilibrium freezing temperature until the droplet is completely frozen. Once frozen, the droplet's temperature once more reduces until it equalizes with the air temperature. It can be seen from Fig. 4 that the thermocouple demonstrated a high sensitivity in detecting the rapid temperature step change at the point of nucleation. The most significant visible changes occurring during the freezing of the droplet represented in Fig. 4 are shown as a series of video frames in Fig. 5. The time positions of each frame are

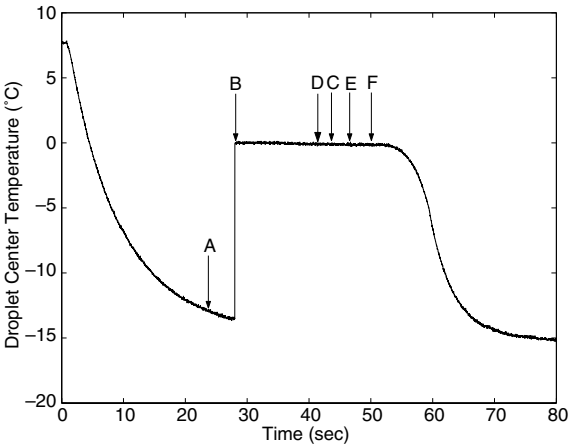

Fig. 4. Temperature profile of a freezing water droplet: $R = 0.78$ mm, $T_a = -15$ °C, $T_n = -13.5$ °C and $v = 0.54\ m\,s^{-1}$.

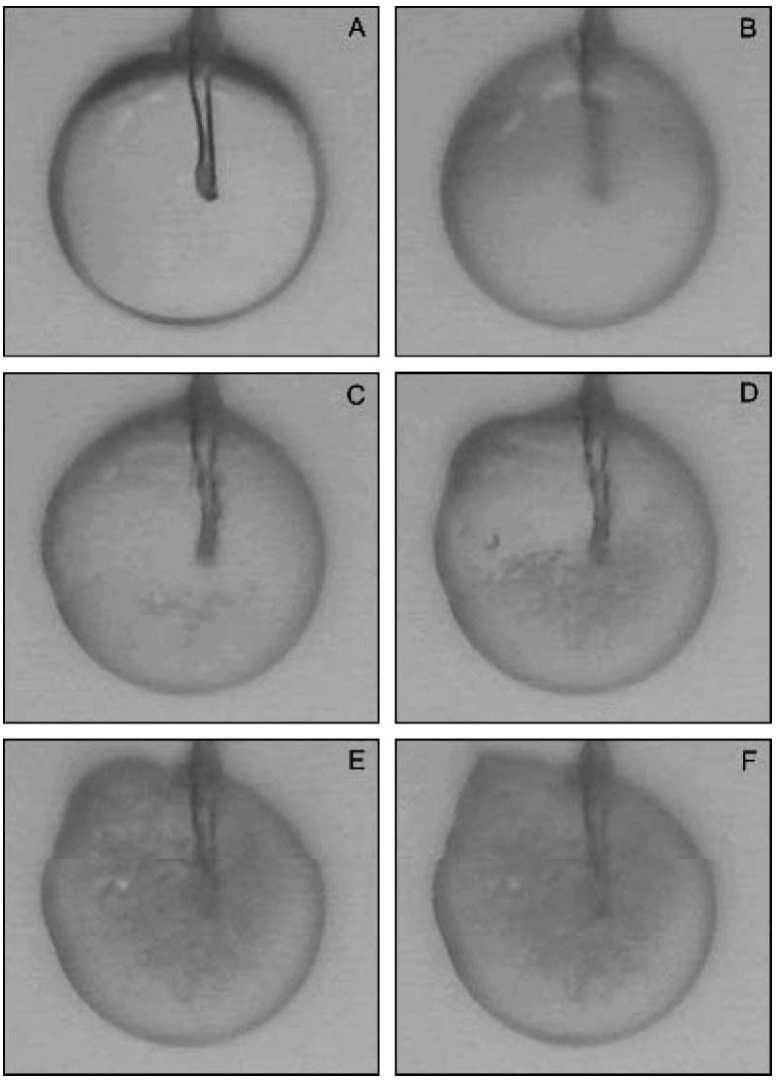

Fig. 5. Video frames of significant observed changes in the droplet freezing in Fig. 4. Time from start of cooling (A) 25 s: supercooled water, (B) 28.5 s: turns opaque immediately after nucleation, (C) 42.5 s: air bubbles first appear (below thermocouple tip), (D) 44.5 s: bulge appears on droplet, (E) 47.5 s: bulge bursts and unfrozen liquid flows onto surface, (F) 50.5 s: final frozen droplet shape, no noticeable change after this time.

given in the legend. At the point of nucleation, the droplet appears to instantly change from clear to opaque (Frames (A) and (B) Fig. 5). The video recorder frame rate of 25 per second was not fast enough to record this transition. It was not possible to observe nucleation location nor the crystal growth structure of the ice formed from the nucleation. The next significant change was the appearance of gas bubbles. In Frame (C) these can be seen just below the tip of the thermocouple. As the droplet continues to freeze the number of bubbles increases and after a period of time a bulge appears at the top of the droplet (Frame (D)). In Frame (E) the bulge has grown until it bursts and liquid flows onto the surface of the droplet. The surface liquid freezes and the final droplet shape is formed by the time of Frame (F). No more changes are observable for the remaining temperature transition of the droplet. These series of observed changes are identical to those seen in the freezing of magnetically levitated water droplets observed by Tagami et al. [29].

The bubbles appeared because air has a much lower solubility in ice than in water so, as ice forms, it rejects the excess gas into the unfrozen liquid. This increases the concentration of dissolved gas in the water until the water becomes supersaturated with dissolved gas. Bubbles will then start to form on the surface of the ice. Due

to surface tension and curvature effects, the presence of bubbles at the solid/liquid interface depresses the freezing point of the water [9]. This would explain the observed downward curving of the temperature profile (after Frame (F)) at the end of the constant temperature freezing stage. Blanchard [38] used the rejection of gas by the ice to explain the droplet turning opaque after nucleation. The scattering of light by minute air bubbles inside the ice formed by the recalescence gives the ice its opaque appearance.

The droplets appear from the video images to nucleate at the surface even with silver iodide present on the thermocouple. This was due to the formation of a solid shell around the droplet. This solid shell was evident by the fact that gas bubbles only appeared at approximately the center of the droplet, whereas no bubbles appeared in the outer part of the droplet. It is therefore presumed that the outer part of the droplet froze first, thus releasing its dissolved gas into an unfrozen center.

Additionally, the formation of a solid shell was evident from the bulging observed at the surface. This was due to the shell being pushed out by a pressure build up inside the droplet from the formation of gas bubbles and the density change of water to ice. Gao et al. [30] videoed the freezing of freely suspended water droplets in a wind tunnel. He was able to observe ice nucleating at the bottom surface and the ice growing to envelop the droplet with the droplet freezing inwardly from an outer shell. It would seem that when the silver iodide was not present, the droplet nucleates at the surface and when it was present, nucleation would occur at the silver iodide (at the thermocouple). In the latter case however, dendrites would rapidly grow out to the surface then grow around the surface to envelope the droplet as the surface region was colder than the body of the droplet.

5.2. Model assessment

The experimental data of 40 droplets frozen at different experimental parameters were collected for the assessment of the model predictions. Assessment of the prediction adequacy of the models was made by calculating the percentage error between the cooling and freezing times predicted by the models and the experimentally measured times. The percentage error was calculated from:

$$\%\text{Error} = \frac{\text{Predicted time} - \text{Experimental time}}{\text{Experimental time}} \times 100$$

Table 3 has a summary of the range of the predicted heat and mass transfer parameters for the range of experimental parameters listed in Table 1. The maximum Reynolds number of 158 means that the air flow around all the droplets was within the laminar flow range. This accounts for the relatively low heat and mass transfer coefficients.

Table 3
Summary of the range of values of heat and mass transfer parameters predicted by the models for the range of experimental parameters in Table 1

Parameter	Min	Max
Droplet Reynolds number *Re*	36	137
Droplet Schmidt number *Sc*	0.485	0.487
Convective heat transfer coefficient h ($\mathrm{J\,s^{-1}\,m^{-2}\,K^{-1}}$)	118	158
Convective mass transfer coefficient h_m ($\mathrm{m\,s^{-1}}$)	0.112	0.152

No data was available for the droplet operating conditions within actual spray freezers. But for counterflow spray dryers the Reynolds numbers range between 30 and 200 [39]. These values are rather low because the mean droplet size is typically 30 μm, so even though the relative droplet to air velocity ranges from 0 to 10 m/s the maximum Reynolds number is close to that used in this study. Therefore, the experimental data and models are likely to be applicable to an operating spray freezer.

5.3. Cooling stages

5.3.1. Liquid cooling stage model selection

The liquid cooling time was the time taken for the droplet to cool from the initial temperature to the nucleation temperature.

The results of the model comparisons are shown as frequency diagrams of the percentage error between the predicted and experimental cooling times in Fig. 6. The

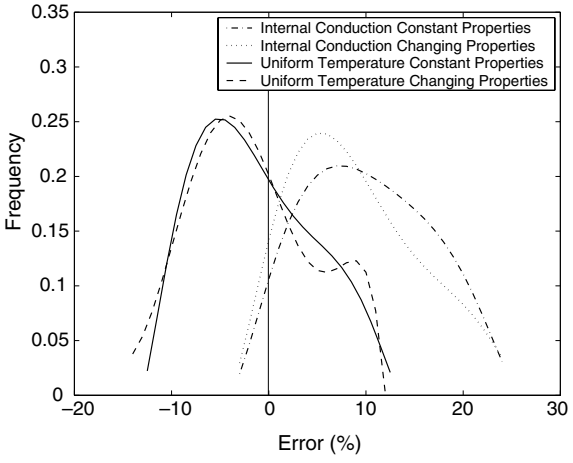

Fig. 6. Frequency diagram of the percentage errors between experimental liquid water cooling times and model predictions, for 40 droplets within the experimental parameter range, see Table 1.

Table 4
Summary of percentage error between experimental and predicted cooling times for liquid water droplets

Model	Mean (%)	Stdev (%)	Conf (±%)
Internal conduction constant properties	8.4	6.5	2.0
Internal conduction changing properties	6.9	6.4	2.0
Uniform temperature constant properties	−3.7	6.1	1.9
Uniform temperature changing properties	−4.6	6.3	2.0

frequency graph gives a visual indication of the spread and overlapping of the results. The mean standard deviation (Stdev) and 95% confidence bounds (Conf) of the percentage error are set out in Table 4 which gives a qualitative indication of the accuracy and repeatability of each model.

The frequency graph in Fig. 6 shows that the addition of changing properties does not significantly change the predicted times for the uniform temperature and internal conduction model even though the mean errors are different by just over 1%. All models have error bounds of 95% confidence, well within the experimental uncertainty of ±6%, so their variations cannot be distinguished from the experimental uncertainty. This indicates that the numerical errors and physical property uncertainties are small compared to the experimental errors.

With the smallest mean error of −3.7%, achieved with the uniform temperature model with constant properties, demonstrates the best prediction capability for the experimental data. Therefore, it was used for the subsequent freezing time predictions. The cooling curves predicted by the uniform temperature model with constant properties showed very good agreement with the experimental data, as can be seen in Fig. 7 for the variation of selected experimental parameters.

Yao and Schrock [15] modelled the cooling of free falling droplets. They also observed that an internal conduction model had the tendency to predict longer cooling times compared with a uniform temperature model. Even though there was a separation of 11% in the mean error between the internal conduction model and the uniform temperature model, the large amount of overlapping seen in the frequency graph means no conclusions can be made on the virtues of using the uniform temperature model compared to the internal heat conduction model.

The models predicted that the contribution of the thermocouple to the total heat transfer from the droplet was <0.1%, for the droplet size range 0.5–2 μl. For the same droplet size range and thermocouple size for

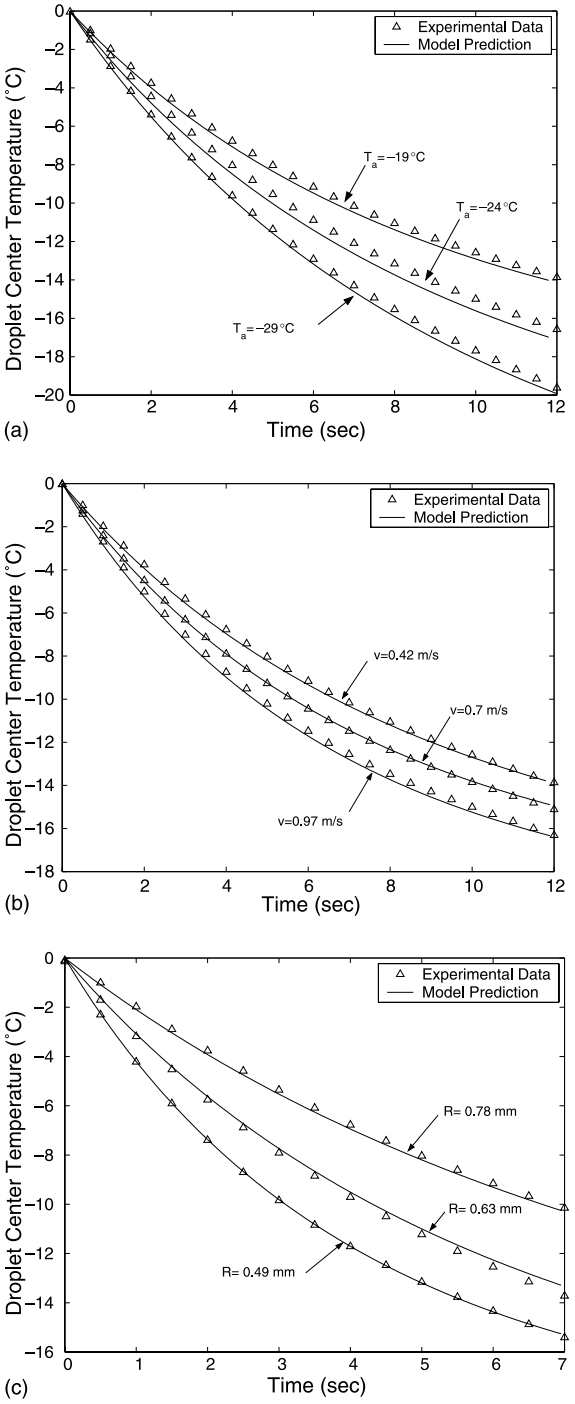

Fig. 7. Liquid cooling stage comparison of uniform temperature model with constant properties with experimental data for the experimental parameters: (a) varying air temperature T_a for $R = 0.78$ mm, and $v = 0.42\ \mathrm{m\,s^{-1}}$; (b) varying air velocity v for $R = 0.78$ mm, and $T_a = -20$ °C; (c) varying droplet radius R, for $v = 0.42\ \mathrm{m\,s^{-1}}$ and $T_a = -20$ °C.

droplet drying experiments Lin and Chen [11] proved experimentally that the conduction of heat through the thermocouple wire was negligible. Therefore, the thermocouple component was neglected from the solid cooling and freezing stage models.

5.3.2. Solid cooling stage model selection

For the model assessment, the solid cooling times were taken as the time from when the droplet temperature was −5 °C after freezing, until it cooled to within 1 °C of the air temperature. This use of −5 °C as a starting point accounted for the observed freezing point depression at the end of the freezing stage.

The uniform temperature model with changing properties was selected for the freezing time predictions. The percentage error frequency graph for each model is detailed in Fig. 8 and summarized in Table 5. From these it can be seen that the uniform temperature model with changing properties was the most accurate model for predicting the cooling times. This had a mean difference of 1.2% and a confidence level of ±1.2%, which indicates that the model was accurate, gave good repeatability and was within the experimental uncertainty. Fig. 9 shows the good performance of the uniform temperature model with changing properties for the variation of several experimental parameters.

The fact that changing properties produced the more accurate predictions of both models was probably due to the significant variation in the heat capacity of the ice at decreasing temperatures (at 0 °C $c_s = 2.116$ whereas at −18 °C $c_s = 1.974$ kJ/kg K [34]). For liquid water, there is comparatively less change in the heat capacity ($c_l = 4.184$ at −18 °C to $c_l = 4.217$ kJ/kg K at 0 °C [34]).

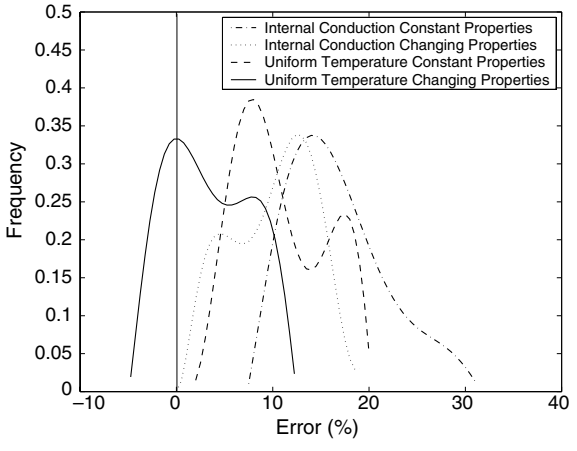

Fig. 8. Frequency diagram of the percentage error between experimental solid water cooling times and model predictions, for 40 droplets within the experimental parameter range, see Table 1.

Table 5
Summary of percentage error between experimental and predicted cooling times for solid water droplets

Model	Mean (%)	Stdev (%)	Conf (±%)
Internal conduction constant properties	14.9	4.9	1.6
Internal conduction changing properties	8.6	4.5	1.4
Uniform temperature constant properties	8.6	4.6	1.4
Uniform temperature changing properties	1.2	3.9	1.2

5.4. Freezing time prediction model selection

The percentage error frequency curves for each numerical model are shown in Fig. 10. The means, standard deviations and confidence bounds are detailed in Table 6.

In the frequency plots it can be seen that the form and spread of each plot are very similar. This indicates that the spread of the data has been produced by the experimental uncertainties and not by the models. This was also shown by the 95% confidence bounds being less than the experimental uncertainties of ±6%. There appears to be a constant time difference in the predictions for each model. This was due to formulation of each model. The solution of the moving boundary only introduces a time lag into the final energy balance of the system. The lag begin the heat conduction through outer region and the changing size of the moving interface, i.e for the inward moving boundary the conduction through a solid with a decreasing interface, whereas, for outward moving boundary conduction through a liquid with a increasing interface. Because of the small size of the droplets these were likely to have been very small as reflected by the small separation of the means of the models.

It can be seen from the results that the outward moving boundary model predicts shorter freezing times than the inward moving boundary model. This trend was also noted with analytical solutions of the inward and outward moving boundaries of the freezing of droplets [35]. It was observed experimentally that the droplets froze inwardly, so, the better performance of the outward moving boundary model would be unexpected. Distinguishing between these models was unimportant because it was unlikely that the freezing occurred as a singular planar front. It was more likely that it would occur by the growth and thickening of dendrite arms, thus, the freezing pattern would be better estimated by the simple heat balance model.

Also, the heat balance model would be a preferable method as it has far less formulation and computational

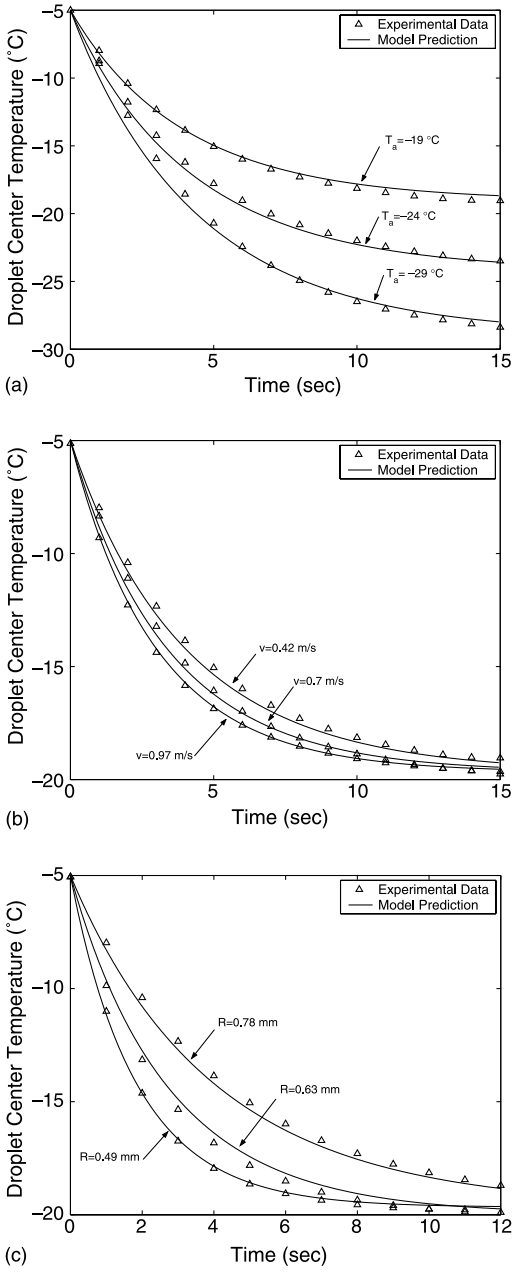

Fig. 9. Solid cooling stage comparison of uniform temperature model with changing properties with experimental data for the experimental parameters: (a) varying air temperature T_a for $R = 0.78$ mm, and $v = 0.42\ m\,s^{-1}$; (b) varying air velocity v for $R = 0.78$ mm, and $T_a = -20$ °C; (c) varying droplet radius R, for $v = 0.42\ m\,s^{-1}$ and $T_a = -20$ °C.

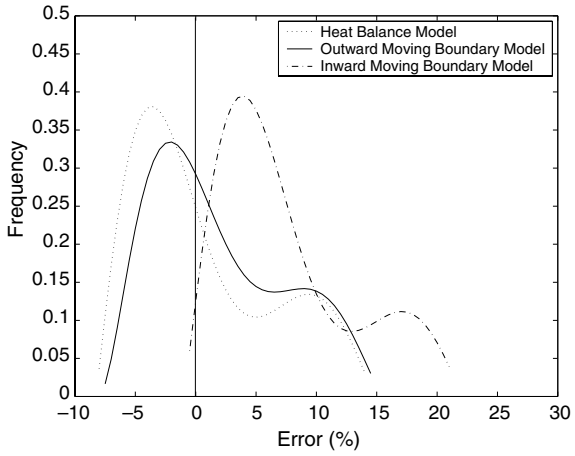

Fig. 10. Frequency diagram of the percentage error between experimental freezing times and numerical model predictions for 40 droplets within the experimental parameter range, see Table 1.

Table 6
Summary of percentage error between experimental and predicted freezing times for water droplets

Model	Mean (%)	Stdev (%)	Conf (±%)
Heat balance	−1.1	5.8	1.8
Outward moving boundary	0.2	5.7	1.8
Inward moving boundary	5.4	6.1	1.9

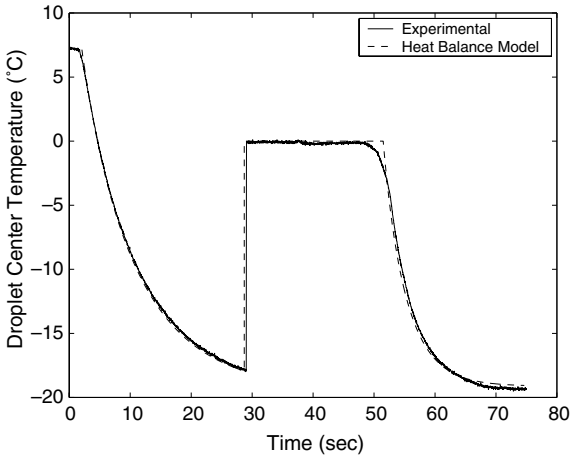

Fig. 11. Comparison of experimental and numerical results for a freezing droplet: $R = 0.78$ mm, $T_a = -19$ °C, $T_n = -18.4$ °C and $v = 0.42\ m\,s^{-1}$.

requirements, while only being slightly less accurate than the outward moving boundary model. Therefore, it was considered the more favorable model to use for freezing time predictions of droplets.

An example of the performance of the complete heat balance model is shown in Fig. 11. The model matches the experimental data very well for the temperature

transition of the freezing droplet, except for the small period of freezing point depression occurring at the end of the freezing stage.

The good accuracy of the model means that heat and mass transfer from the droplet was well described. This shows that the Ranz and Marshall correlations can be extended to sub-zero temperatures. Also, the recalescence model was very good at estimating the frozen volume produced from relief of supercooling.

5.5. Effect of nucleation temperature

The nucleation temperature range of pure distilled water (without silver iodide present on the thermocouple) for this study was −18 to −21 °C, with a mean temperature of −19 °C. This agrees well with the mean nucleation temperature of −21 °C found by Biggs (quoted by Hobbs [9]) for distilled water droplets of a similar radius (0.78 mm). Biggs froze the droplets which were suspended at the interface of two immiscible liquids. This suggests that the thermocouple has only a small nucleating effect. The nucleation temperature of the droplets nucleated with silver iodide ranged from −3.5 to −15 °C.

The effect the nucleation temperature has on the freezing time for two different air temperatures is shown in Fig. 12. The graph shows that the freezing time was only significantly influenced by the nucleation temperature if the air temperature was set close to the minimum nucleation temperature. This occurs because the driving force for the heat transfer decreases as the droplet temperature approaches the air temperature. Thus, the cooling time was increased before the droplet nucleated whereas there was little benefit gained from increasing the supercooling which would increase the frozen volume produced from the recalescence.

If the air temperature is higher than the nucleation temperature, the droplet will remain supercooled for an indefinite amount of time before it nucleates. This would then greatly increase the freezing time. Therefore, the nucleation characteristics of the material must be well known to optimally set the air temperature for a spray freezer.

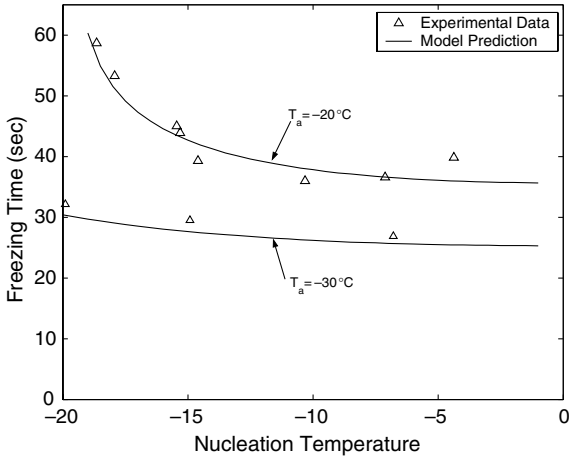

Fig. 12. Influence of nucleation temperature on freezing time for different air temperatures T_a with $R = 0.78$ mm and $v = 0.42$ m s^{-1}. Solid lines show freezing times predicted by heat balance model.

6. Conclusions

An experimental and numerical analysis was performed on the freezing of a droplet of distilled water. A simple experimental apparatus based on suspending a single droplet on a thermocouple junction was able to effectively measure the temperature and observe the freezing of the droplet. All the stages of the freezing process could be clearly observed. The phenomenon of freezing point depression of the water was observed. This was caused by gas bubbles formed by the release of dissolved gas from the unfrozen liquid at the solid/liquid interface. After recalescence, water droplets turned opaque by the formation of a solid shell with an unfrozen center, even when the droplet was forced to nucleate at the center by silver iodide fixed on the thermocouple.

All of the numerical models used gave a reasonable prediction of the experimental freezing times. A simple heat balance model for each of the liquid cooling, solid cooling and freezing stages was sufficient for the purpose of solving the internal energy balance of the droplet, giving accurate results well within the experimental uncertainty. The solid cooling stage accuracy was increased with the addition of changing thermal properties.

The accuracy of the models meant that the correlations developed by Ranz and Marshall [31] showed good applicability to dual heat and mass transfer from a spherical object at sub-zero temperatures.

The models developed here show potential for design and optimization of spray freezing applications. Incorporation of solute techniques would be necessary for prediction of the behaviour of real fluids of interest. This will be the subject of further study.

References

[1] E. Windhab, New developments in crystallization processing, J. Thermal Anal. Calorimetry 57 (1999) 171–180.
[2] J. Berriman, N. Unwin, Analysis of transient structures by cryo-microscopy combined with rapid mixing of spray droplets, Ultramicroscopy 56 (1994) 241–252.

[3] N. El-Kaddah, J. Szekely, The electromagnetic force field, fluid flow field, and temperature profiles in levitated droplets, Metall. Trans. B 14B (1983) 401–410.
[4] S. Song, B. Li, Free surface profiles and thermal convection in electrostatically levitated droplets, Int. J. Heat Mass Transfer 43 (2000) 3589–3606.
[5] B. Adhikari, T. Howes, B. Bhandari, V. Truong, Experimental studies and kinetics of single drop drying and their relevance in drying of sugar-rich foods: a review, Int. J. Food Properties 3 (2000) 323–351.
[6] N. Roth, A. Frohn, Size and polarization behaviour of optically levitated frozen water droplets, Atmos. Environ. 32 (1998) 3139–3143.
[7] S. Song, B. Li, A boundary/finite element analysis of magnetic levitation systems: surface deformation and thermal phenomena, Trans. ASAE 120 (1998) 492–504.
[8] A. Trommelen, E. Crosby, Evaporation in drying of droplets and superheated vapours, AIChE J. 16 (1970) 857–866.
[9] P. Hobbs, Ice Physics, Oxford University Press, London, 1974.
[10] L. Hallett, Experimental studies of the crystallisation of supercooled water, J. Atmos. Sci. 21 (1964) 671–682.
[11] S. Lin, X. Chen, The micro-world of drying of milk droplets part 1: single droplet drying kinetics, in: 6th World Congress of Chemical Engineering, Melbourne, Australia, 2001.
[12] M. Epstein, H. Fauske, Kinetic and heat transfer-controlled solidification of highly supercooled droplets, Int. J. Heat Mass Transfer 36 (12) (1993) 2987–2995.
[13] E. Brunier, C. Jolivet, P. Guigon, D. Clausse, Solidification of supercooled spherical droplets, in: Numerical Methods in Thermal Problems, Proceedings of the Seventh International Conference, Stanford, USA, Pineridge Press, Swansea, UK, 1991, pp. 291–301.
[14] O. Miyawaki, T. Abe, T. Tano, A numerical model to describe freezing of foods when supercooling occurs, J. Food Eng. 9 (1989) 143–151.
[15] S. Yao, V. Schrock, Heat and mass transfer from freely falling drops, J. Heat Transfer, Trans. ASME Ser. C 98 (1) (1976) 120–126.
[16] J. Liao, K. Ng, Effect of ice nucleators on snow making and spray freezing, Ind. Eng. Chem. Res. 29 (3) (1990) 361–366.
[17] V. Alexiades, D. Solomon, Mathematical Modeling of Melting and Freezing Processes, Hemisphere Publishing Corporation, Washington, DC, 1993.
[18] W. Murry, F. Landis, Numerical and machine solutions of transient heat-conduction problems involving melting or freezing, Trans. ASME J. Heat Transfer 81 (1959) 106–112.
[19] V. Voller, Implicit finite-difference solutions of the enthalpy formulation of Stefan problems, J. Numer. Anal. 5 (1985) 201–214.
[20] J. Caldwell, C. Chan, Spherical solidification by the enthalpy method and the heat balance integral method, Appl. Math. Model. 24 (2000) 45–53.
[21] A. Bonacina, Numerical solution of phase-change problems, Int. J. Heat Mass Transfer 16 (1973) 1825–1832.
[22] G. Wang, E. Matthys, Numerical modeling of phase change and heat transfer rapid solidification processes: use of control volume integrals with element subdivision, Int. J. Heat Mass Transfer 35 (1992) 141–153.
[23] A. Wheeler, N. Ahmad, Recent developments in phase-field models of solidification, Adv. Space Res. 16 (7) (1995) 163–172.
[24] A. Delgado, D.-W. Sun, Heat and mass transfer models for predicting freezing processes—a review, J. Food Eng. 47 (2001) 157–174.
[25] C. Levi, R. Mehrabian, Heat flow in atomized droplets, Metall. Trans. B 11B (1980) 21–27.
[26] H. Wilson, R. Singh, Numerical simulation of individual quick freezing of spherical foods, Rev. Int. Froid 10 (1987) 149–155.
[27] G. Wang, V. Prasad, E. Matthys, An interface tracking numerical method for rapid planar solidification of binary alloys with application to microsegregation, Mater. Sci. Eng. A 225 (1997) 47–58.
[28] R. Kobayashi, Modeling and numerical simulations of dendritic crystal growth, Physica D 63 (1993) 410–423.
[29] M. Tagami, M. Hamai, I. Mogi, K. Watanabe, M. Motokawa, Solidification of levitating water in a gradient strong magnetic field, J. Cryst. Growth 203 (1999) 594–598.
[30] W. Gao, D. Smith, D. Sego, Freezing behavior of freely suspended industrial waste droplets, Cold Regions Sci. Technol. 31 (2000) 13–26.
[31] F. Incropera, D. DeWitt, Fundamentals of heat and mass transfer, fourth ed., John Wiley and Sons, New York, USA, 1996.
[32] A. Kucherov, Sublimation and vaporization of an ice aerosol particle in the form of thin cylinder by laser radiation, Int. J. Heat Mass Transfer 43 (2000) 2793–2806.
[33] D. Lide, CRC Handbook of Chemistry and Physics, 80th ed., CRC Press, Boca Raton, FL, 1999.
[34] R. Perry, D. Green, Perry's Chemical Engineer's Handbook, seventh ed., McGraw-Hill, New York, 1997.
[35] F. Feuillebois, A. Lasek, P. Creismeas, F. Pigeonneau, A. Szaniawski, Freezing of a subcooled liquid droplet, J. Colloid Interface Sci. 169 (1995) 90–102.
[36] X. Chen, P. Chen, Freezing of aqueous solution in a simple apparatus designed for measuring freezing point, Food Res. Int. 29 (8) (1996) 723–729.
[37] D. Cleland, R. Earle, A comparison of methods for predicting the freezing times of cylindrical and spherical foodstuffs, J. Food Sci. 44 (1979) 958–963.
[38] D. Blanchard, The supercooling freezing and melting of giant water drops at terminal velocity in air, in: O. Institute (Ed.), Artificial Stimulation of Rain Proceedings of the First Conference on the Physics of Clouds and Precipitation Particles, Pergamon, New York, 1955, pp. 233–249.
[39] T. Langrish, D. Fletcher, Spray drying of food ingredients and applications of cfd in spray drying, Chem. Eng. Process. 40 (2001) 345–354.
[40] E. Dorsey, Properties of Ordinary Water-substance, Reinhold Publishing Corporation, New York, USA, 1940.